Biosensors and Bioelectronics 26 (2011) 4012–4017

Contents lists available at ScienceDirect

Biosensors and Bioelectronics

journal homepage: www.elsevier.com/locate/bios

Electrochemical measurement of the flux of hydrogen peroxide releasing from RAW 264.7 macrophage cells based on enzyme-attapulgite clay nanohybrids

Ping Wu [a], Zhewei Cai [a,1], Jing Chen [b], Hui Zhang [a], Chenxin Cai [a,*]

[a] Jiangsu Key Laboratory of New Power Batteries, Jiangsu Key Laboratory of Biofunctional Materials, Laboratory of Electrochemistry, College of Chemistry and Materials Science, Nanjing Normal University, Nanjing 210097, PR China

[b] Jiangsu Provincial Key Laboratory of Palygorskite Science and Applied Technology, College of Bioengineering and Chemical Engineering, Huaiyin Institute of Technology, Huaian 223003, PR China

ARTICLE INFO

Article history:
Received 27 January 2011
Received in revised form 18 March 2011
Accepted 19 March 2011
Available online 26 March 2011

Keywords:
Electrocatalysis
Biotechnology
Attapulgite
Hydrogen peroxide
Macrophage cells

ABSTRACT

Determination of cellular ROS (reactive oxygen species) could lead to a better understanding of the clinical consequences of the enhancement in ROS concentration, and assisting in studies of the biological effect of ROS in cells. This work developed an electrochemical approach for measuring the flux of H_2O_2 (a major ROS in living organisms) releasing from RAW 264.7 macrophage cells. This approach is based on the electrocatalytic reduction of the releasing H_2O_2 at the biosensor of HRP-attapulgite/GC, which was fabricated by depositing the horseradish peroxidase-attapulgite nanohybrids on the glassy carbon (GC) electrode. The biosensor exhibited a rapid response, a wide linear range, a high sensitivity, a low detection limit, as well as good stability and repeatability due to using the natural mineral (attapulgite) as the enzyme immobilization substrate. In addition, some common coexisting ROS and compounds in biological system such as hypochlorite (OCl^-), nitric oxide ($NO^\bullet$), peroxynitrite ($ONOO^-$), and ascorbic acid (AA) etc., did not cause any interference due to the use of a low operating potential (−400 mV, versus SCE). Moreover, the developed approach can also be used for studying the effects of the stimulator loading and a variety of stimuli on the generation of H_2O_2 in cells and the release flux of H_2O_2 from cells. Therefore, this work has demonstrated a simple and effective sensing platform for detection of cellular H_2O_2 released from cells such as RAW 264.7 cells, which has potential utility to cellular biology and pathophysiology.

1. Introduction

In biology, signal transduction initiated by complex protein–protein interactions between ligands, receptors, and kinases is a mechanism that converts a mechanical/chemical stimulus to a cell into a specific cellular response (Simons and Toomre, 2000). It has become increasingly evident that reactive oxygen species (ROS) including superoxide anion ($O_2^{\bullet -}$), hydroxyl radical ($^\bullet OH$), hydrogen peroxide (H_2O_2), hypochlorous acid (HOCl), and peroxynitrite ($ONOO^-$), etc.) participate in the signal transduction processes in a concentration dependent manner (Finkel, 2000). At a low concentration, they act as a second messenger in cellular signal transduction and signal amplification, playing an important role as the regulator for a number of oxidative stress-related states. Whereas at a high concentration, they can damage major cellular constituents and harm to living organisms, causing a number of pathological events ranging from aging (Droge and Schipper, 2007), neurodegeneration (DiMauro and Schon, 2008), to cancer (Finkel et al., 2007; Rossi et al., 2008). Therefore, the quantitative determination and mediation of cellular ROS concentration could lead to a better understanding of the clinical consequences of the enhancement in ROS concentration as well assisting in studies designed to elucidate the biological effect of ROS in cells.

H_2O_2, a major ROS in living organisms, affects cell proliferation and cell death (Chang et al., 2004), leading to the diverse downstream biological effects connected with lipid peroxidation (Sevanian and Hochstein, 1985), DNA damage (Troll and Wiesner, 1985), tumor promotion (Ohshima et al., 2003), etc. It is the most common representative of ROS studied in cellular environments due to its stability and penetration through cellular membranes. A variety of techniques, including colorimetry (Kojima et al., 1998), electrochemical methods (Luo et al., 2009; Li et al., 2010), chemiluminescence (Wang et al., 2010; Ye et al., 2010), and fluorescence (Miller et al., 2007; Dickinson et al., 2010; Kim et al., 2010), electron spin resonance (Bartosz, 2006), etc., have been developed for analyzing cellular H_2O_2. Among these methods, enzyme-based

* Corresponding author. Tel.: +86 25 85891780; fax: +86 25 85891767.
E-mail address: cxcai@njnu.edu.cn (C. Cai).

[1] Student of Jinling High School (Nanjing, China) and currently conducting a project of innovation study in Nanjing Normal University.

0956-5663/$ – see front matter © 2011 Elsevier B.V. All rights reserved.
doi:10.1016/j.bios.2011.03.018

electrochemical biosensors have received considerable attention and become an attractive method for in vivo and ex vivo biological application. Moreover, compared with other methods, the biosensor can offer the direct, rapid, and real-time measurements with no need for using the poor stability and easy photobleaching fluorescent probe molecule, adding chemiluminescence reagents, or detecting under rigorous environment conditions (Xu et al., 2002; Chen et al., 2010; Wu et al., 2010).

Generally, enzyme-based biosensors are developed by immobilizing enzymes on the surface of the suitable materials or on the electrode surface because the direct use of enzymes in solution suffers the poor stability (Meng et al., 2009a; Miao et al., 2010). To keep the intrinsic secondary structure of the enzyme and enhance the efficiency of the biosensor, it is critical to choose a biocompatible material for immobilizing the enzymes. Attapulgite, a natural nanostructure clay, was employed in this work as an enzyme immobilization material to develop a H_2O_2 biosensor. Attapulgite has a special laminated chain structure with specific fibrous morphology, high surface area, good thermal resistance, moderate absorptive capacity, and fine biological affinity, providing much potential for diverse applications such as catalyst supports, nanocomposites, pharmaceutical industry and environmental absorbents (Yang et al., 2010). However, there are few reports concerning the use of this natural mineral for the assembly of the enzymes. Horseradish peroxidase (HRP) was selected as a model enzyme to fabricate the H_2O_2 enzyme-based biosensor due to its high electrocatalytic activity toward the reduction of H_2O_2, known structure, and commercial availability (Cai and Chen, 2004; Peng et al., 2009; Shan et al., 2010). The preparation and characteristics of the HRP-attapulgite biosensor are presented herein. The monitoring the flux of H_2O_2 released from RAW 264.7 macrophage cells using the biosensor is also demonstrated.

2. Experimental

2.1. Chemicals

Horseradish peroxidase (HRP, E.C. 1.11.1.7, Type VI, lyophilized powder, 250–330 U mg^{-1}, Sigma), catalase (E.C. 1.11.1.6, from bovine liver, lyophilized powder, 2000–5000 U mg^{-1}, Sigma), phorbol 12-myristate 13-acetate (PMA, ~99%, Sigma), *N*-formylmethionyl-leucylphenylalanine (fMLP, ≥97%, Sigma), adenosine 5′-diphosphate (ADP, ≥95%, Sigma), ascorbic acid (AA, ≥99.0%, Sigma), 3-(aminopropyl)-1-hydroxy-3-isopropyl-2-oxo-1-triazene (NOC-5, Sigma), and 3-morpholinosydnonimine (SIN-1, Sigma) were used as received. Prior to use, attapulgite (Jiuchuan Clay Company, Xuyi, China) was treated according to the reported procedures (Yang et al., 2010). Solutions of H_2O_2 were freshly diluted from the 30% solution, and their concentrations were determined using a standard $KMnO_4$ solution. 0.1 M phosphate buffer solution (PBS, pH 7.4) was employed as the supporting electrolyte. All other chemicals were of analytical grade. All solutions were prepared with double distilled water.

2.2. Instruments and procedures

Transmission electron microscopic (TEM) images were obtained with a JEOL-2010 transmission electron microscope operating at an accelerating voltage of 120 kV. UV–vis spectra were recorded using a Cary 5000 UV–vis-NIR spectrophotometer (Varian, USA). Circular dichroic (CD) measurements were made on CD Chirascan (Applied Photophysics Ltd.) in a 1 cm quartz cuvette. The FT-IR spectrum was recorded on a Nexus 670 FT-IR spectrophotometer (Nicolet Instruments) using a KBr disk at a resolution of 4 cm^{-1}. The value of Zeta potential (ζ) of the attapulgite nanostructures was measured using a Zeta potential analyzer (Zetasizer Nano, Malvern).

The electrochemical experiments were performed with a CHI 760B electrochemical workstation (CH Instruments). A two-compartment three-electrode cell with the sample volume of 10 mL was employed. A coiled Pt wire and a saturated calomel electrode (SCE) were used as the counter electrode and the reference electrode, respectively. Buffers were purged with high purity nitrogen for at least 30 min prior to experiments and the nitrogen environment was then kept over the solution to prevent oxygen from reaching the solution. Amperometric measurements were performed under a constant potential of −400 mV (versus SCE). The solution was continuously stirred using a magnetic bar at a rate of 250 rpm.

2.3. Assembly of HRP on attapulgite and fabrication of HRP-attapulgite/GC electrode

Several experimental parameters were optimized to obtain the best voltammetric response. For immobilization of HRP, attapulgite powder (2 mg) was dispersed into HRP solution (1 mL, 5 mg mL^{-1} in pH 7.4 PBS) by continuously stirring at 4 °C for 2 h. After that, the mixture was centrifuged and the HRP-attapulgite nanohybrids were collected by removing the supernatant. The nanohybrids were thoroughly washed with PBS to remove the loosely assembled enzyme molecules.

To fabricate the HRP-attapulgite/GC electrode, the HRP-attapulgite nanohybrid was dispersed into PBS (pH 7.4) to form a homogeneous suspension (5 mg mL^{-1}). Then, the suspension (5 μL) was cast onto the surface of the glassy carbon (GC, 3 mm in diameter, CH Instruments) electrode with a microsyringe, and solvent was allowed to be evaporated before use. The HRP-attapulgite/GC electrode was stored at 4 °C when not in use.

By similar procedures, the attapulgite/GC and HRP/GC electrodes were also fabricated, and their electrocatalytic characteristics were compared with those of the HRP-attapulgite/GC electrode.

2.4. Cell culture

RAW 264.7 macrophage cells were grown at 37 °C in DMEM (Dulbecco's Modified Eagle Medium) supplemented with 10% (v/v) fetal bovine serum (FBS), 100 U mL^{-1} penicillin, and 100 mg mL^{-1} streptomycin in a 5% CO_2 environment. After growing to 90% confluence, the cells were then washed three times with PBS (0.145 M NaCl, 1.9 mM NaH_2PO_4, 8.1 mM K_2HPO_4, pH 7.4) and the cell number was estimated by a hemocytometer.

2.5. Measuring the flux of H_2O_2 releasing from RAW 264.7 cells

The release flux of H_2O_2 from RAW 264.7 cells was measured with the use of the HRP-attapulgite/GC electrode. RAW 264.7 cells (~1×10^7 cells) were centrifuged to obtain a cell-packed pellet with diameter of ca. 0.5 cm and 1 mL PBS was added for the electrochemical experiments. Before measurements, the buffer was deoxygenated by gently shaking the cells under a humidified nitrogen stream. The HRP-attapulgite/GC electrode, which was carefully adjusted to near the cell pellet under a microscope (AxioObserver A1, Carl Zeiss), was biased at −400 mV (vs. SCE). After a steady state background was attained, 100 μL PMA (with the final concentration of 100 ng mL^{-1}) was injected into buffer, and response current corresponding to the electrocatalytic reduction of H_2O_2 releasing from the cells was recorded under the physiological pH and temperature (pH 7.4 and 37 °C). PMA is a well-established ROS stimulator to induce the production of H_2O_2 in macrophages by activating protein kinase C (PKC)

and triggering respiratory burst (Amatore et al., 2008; Lin et al., 2008).

The effects of PMA concentration on the release of H_2O_2 from the cells were also evaluated. Various concentrations of PMA (ranging from 50 to 400 ng mL^{-1}) were injected into the buffer to induce the generation of H_2O_2 in the cells, and the flux of H_2O_2 from the cells was measured using the developed electrode.

To study the stimulus type-dependent characteristics of the H_2O_2 releasing from the RAW 264.7 cells, fMLP, ADP, and AA was added into the buffer, respectively, with each concentration of 400 ng mL^{-1}. fMLP, ADP, and AA have also been demonstrated to be able to induce the generation of H_2O_2 in the RAW 264.7 cells (He et al., 2008; Kim et al., 2010). The release process and the release flux of H_2O_2 were monitored by recording the change of the reduction current of H_2O_2 at the electrode with time.

3. Results and discussion

3.1. Assembly of HRP on attapulgite surface

The mineral attapulgite, a hydrated magnesium silicate, consists of a double chain of Si–O tetrahedral running parallel to the long axis. Upper and lower parts of each double chain are linked by a layer of octahedral magnesium atoms in 6-fold coordination. The chains form a network of strips that are joined together only along the edges. Significantly, the natural mineral has a variable composition because of partial replacement of magnesium by aluminum, iron, calcium, and other elements (Yang et al., 2010). The TEM image indicates that the nanostructures have a needle-like morphology with an average size of 20–50 nm in width and 0.5–1 μm in length (Fig. S1, Electronic Supplementary Information, ESI). They can be individually separated and uniformly distributed on the electrode surface. This feature is very useful for the nanostructures being used for substrate to immobilize the enzymes because the uniform nanostructure can significantly increase the effective surface of the electrode and enhance the enzymes loading and therefore, improving the electrochemical response. The isoelectric point of attapulgite is 4–4.5 (Neaman and Singer, 2000), suggesting that the nanostructures have a net negative surface charge in PBS (pH 7.4). This can be further verified by the analysis of Zeta potential (ζ) since the value of ζ for the nanostructures is ca. −(28 ± 2) mV. HRP is positively charged in pH 7.4 PBS because its isoelectric point of the enzyme is ca. 8.9 (Welinder, 1979). Therefore, HRP could be assembled on the negative charged surface of attapulgite based on electrostatic interaction forming the HRP-attapulgite nanohybrids as verified by UV–vis spectra (Fig. 1). The UV–vis spectrum of attapulgite shows a feature-less curve (curve a, panel A, Fig. 1), however, HRP-attapulgite shows the Soret band at 403 nm (curve c, panel A, Fig. 1), indicative of the effective assembly of HRP on the attapulgite nanostructures. The features of the peak are identical with those of native HRP dissolving in solution (403 nm, curve b, panel A, Fig. 1), demonstrating that no significant denaturation occurred to the enzyme after being assembled onto the surface of the nanostructures.

This conclusion can be further supported by CD spectra. The spectrum in the far-UV region (200–250 nm) corresponds to the peptide $n \rightarrow \pi^*$ electronic transition and it is sensitive to the conformational changes of proteins (Carlsson et al., 2005). The spectra of HRP aqueous solution in this region exhibit two negative peaks at ca. 207 and 222 nm (curve a, panel B, Fig. 1), respectively, which are the characteristic features of heme proteins (Xhattopadhyay and Mazumdar, 2000; Meng et al., 2009b). The CD spectrum of

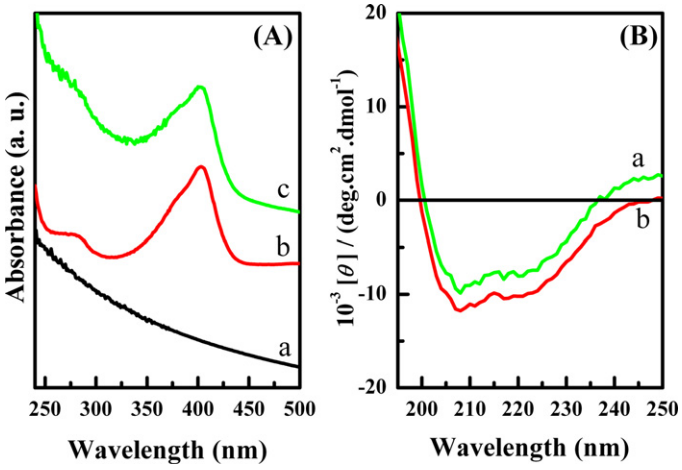

Fig. 1. Panel A: UV–vis spectra of attapulgite nanostructures (a), HRP in solution (0.5 mg mL^{-1} (b), and the HRP-attapulgite nanohybrids (c). Panel B: CD spectra of HRP in solution (a) and HRP-attapulgite nanohybrids (b) in the far-UV region. Curve (a) is displayed by two units' shifts for clarity.

HRP-attapulgite (curve b, panel B, Fig. 1) in this region is also characterized by two negative peaks, whose positions are almost the same as those depicted in curve a (panel B), indicating that the structure and the conformation of HRP after being confined on the surface of attapulgite nanostructures are essentially the same as those in its natural state. This conclusion is also verified by IR spectra presented in Fig. S2 (Electronic Supplementary Information, ESI). These results show good biocompatibility of the attapulgite nanostructures.

3.2. Electrocatalytic reduction of H_2O_2 at the HRP-attapulgite/GC electrode

The aim of this work is to develop a biosensor for monitoring the release process and measuring the flux of H_2O_2 from cells. To evaluate the possibility of the biosensor used in this purpose, the voltammetric responses of the HRP-attapulgite/GC electrode toward the reduction of H_2O_2 were studied. At the absence of H_2O_2, the voltammetric response of the electrode is characterized by a pair of well-defined redox peak with the cathodic (E_{pc}) and anodic (E_{pa}) peak potential of ca. −350 and −300 mV (at 100 mV s^{-1}, in N_2-saturated PBS), respectively (curve a, panel A, Fig. 2), which can be ascribed to the direct electron transfer (DET) reaction of HRP assembled on the nanostructures (Huang and Tsai, 2009; Wang et al., 2009; Yang et al., 2008) (please refer to detailed analysis presented in the ElectronicSupplementary Information, ESI, Fig. S3). This result indicates that attapulgite can facilitate the effective DET between HRP and the electrode surface in spite of the large molecular structure of HRP.

Upon addition of H_2O_2 (0.2 mM), the shape of the cyclic voltammogram of the electrode changes significantly, being characterized by a large cathodic peak at ca. −410 mV (curve b, panel A) and complete disappearance of the anodic peak. The increase of H_2O_2 concentration leads to the enhancement of the cathodic current (not shown here). These characteristics are the typical features of electrocatalytic reactions. The reduction of H_2O_2 starts at a potential of ca. −100 mV, and the observed reduction current increases quite rapidly during negative potential scanning and reaches the highest catalytic current at ca. −410 mV. The results presented in panels B, C, and D (Fig. 2) show that the reduction current can only be observed at the potential more negative than −400 mV, demonstrating that electrocatalytic activity of bare GC, attapulgite, or HRP immobilized on the GC electrode toward the reduction of H_2O_2 is low. Therefore, it can be concluded that HRP-attapulgite nanohybrids presents a good electrocatalyst for the reduction of H_2O_2,

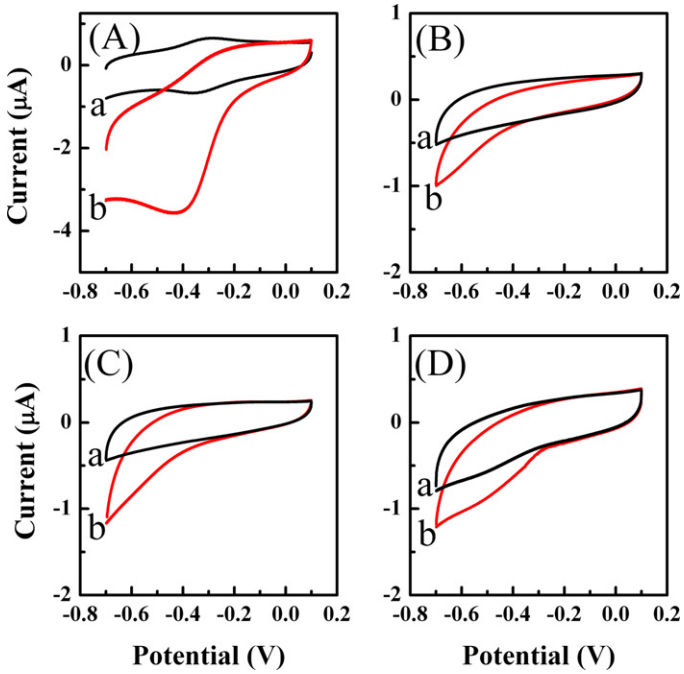

Fig. 2. Voltammetric responses of the HRP-attapulgite/GC (panel A), bare GC (panel B), attapulgite/GC (panel C), and HRP/GC electrodes (panel D) in N_2-saturated PBS (0.1 M, pH 7.4) with (curve b) and without (curve a) 0.2 mM H_2O_2. Scan rate was 100 mV s^{-1}.

indicating that HRP assembled on the attapulgite nanostructures retains its intrinsic and good electrocatalytic activities toward its substrates. The postulated elecrocatalytic mechanism involving in this case is based on DET between HRP and the electrode surface. Such an electrochemical behaviour could be consistent with the following reactions (Cao et al., 2008; Gorton et al., 1992; Lindgren et al., 2000; Ledru et al., 2006):

$$\text{HRP-(Fe}^{\text{III}}\text{)} + \text{H}_2\text{O}_2 \rightarrow \text{Compound-I} + \text{H}_2\text{O} \quad (1)$$

$$\text{Compound-I} + \text{e}^- \rightarrow \text{Compound-II (at electrode)} \quad (2)$$

$$\text{Compound-II} + 2\text{H}^+ + \text{e}^- \rightarrow \text{HRP-(Fe}^{\text{III}}\text{)} + \text{H}_2\text{O (at electrode)} \quad (3)$$

The protein contains the heme as active site and the heme-iron oxidation state is Fe^{III} in the resting state. The catalytic reaction starts on the rapid reaction of HRP-(Fe^{III}) with H_2O_2 to produce an oxidized form, called compound-I, in which the active site contains an oxyferryl center ($Fe^{IV}=O$) and a porphyrin $\pi-$cation radical. The compound-I can get one electron from electrode to produce compound-II, an intermediate form of HRP. The compound-II can further be reduced at the electrode surface to regenerate the HRP-(Fe^{III}) ground state, forming a catalytic cycle.

Fig. 3 depicts the typical steady state amperometric response of the HRP-attapulgite/GC electrode to the successive addition of H_2O_2 in PBS (pH 7.4) solution at a detection potential of −400 mV, which was selected by considering the voltammetric response of H_2O_2 at the electrode and the noise at different detection potentials (Fig. S4, Electronic Supplementary Information, ESI). Immediately after the addition of H_2O_2, the response increases and reaches 95% of the steady state value within ca. 2 s. The response time is shorter than those obtained at other electrodes (Table S1, Electronic Supplementary Information, ESI), suggesting that the electrode responds rapidly to the change of the substrate concentration. The electrode linearly responds to H_2O_2 at lower concentration and attains a saturation level at a higher concentration, representing a typical Michaelis–Menten enzymatic reaction characteristic (inset A, Fig. 3). The response displays a good linear range from

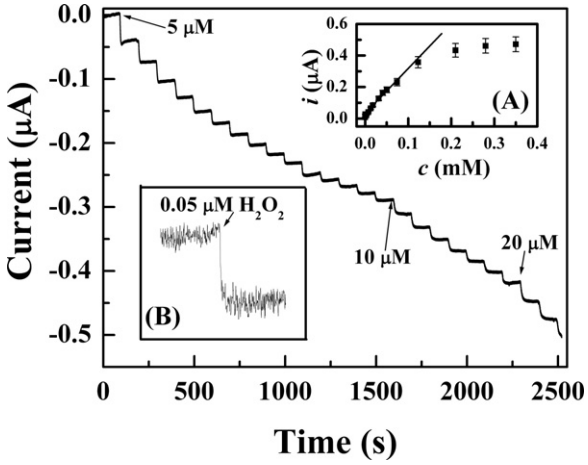

Fig. 3. Amperometric responses of the HRP-attapulgite/GC electrode to the successive addition of H_2O_2 in PBS (0.1 M, pH 7.4) at an applied potential of −400 mV. The insets show the dependence of the response of the electrode on H_2O_2 concentration under the optimal conditions (inset A), and the relationship of the signal-to-noise ratio at S/N of 3 (inset B).

0.2 to 150 μM with a correlation coefficient of 0.997 and a slope of (3.8 ± 0.2) μA mM^{-1}. Therefore, the sensitivity is calculated to be (55.8 ± 2.9) μA mM^{-1} cm^{-2}. The apparent Michaelis–Menten constant (K_M^{app}) is estimated to be (0.09 ± 0.02) mM. The detection limit is estimated to be ca. (0.05 ± 0.01) μM (at a signal/noise of 3, inset B, Fig. 3), which is much lower than those reported previously (Table S1, Electronic Supplementary Information, ESI). Therefore, it can conclude that the value of K_M^{app} is much lower than those previous reported models (Table S1, Electronic Supplementary Information, ESI), implying that attapulgite can provide a good biocompatible microenvironment for maintaining enzymatic activity. This is an advantage of the developed biosensor compared with those reported previously.

The selectivity and anti-interference advantages of the biosensor are demonstrated by recording the response of some common coexisting ROS and compounds in biological system such as OCl^-, $NO^•$, $ONOO^-$, and AA, at the biosensor and compared with that of H_2O_2 (Fig. S5, Electronic Supplementary Information, ESI). While a well-defined H_2O_2 response is observed at the biosensor, biological relevant ROS and compounds result a negligible signal, largely due to the use of low operating potential in the detection. Further results demonstrate that there is an acceptable repeatability in the construction of the biosensor and a good stability in the detection of H_2O_2 (please refer to the evaluation of the repeatability, assay precision, and stability of the electrode in Electronic Supplementary Information, ESI). Hence, a highly selective response to H_2O_2 is obtained without the use of a perm-selective membrane or enzymatic preoxidation. This is another advantage of the developed biosensor. These results indicate that the suitability of the biosensor to monitor the release process and measure the flux of H_2O_2 from cells.

3.3. *Measuring the flux of H_2O_2 releasing from RAW 264.7 cells*

Macrophages are key cells in the immune system playing an important role in host protection against a wide range of tumors and microorganisms by phagocytosis, antigen presentation, and the production of cytokines, nitrogen species (RNS), and ROS involved in the destruction of pathogens (Amatore et al., 2010). When the cells were stimulated, respiratory burst occurred with H_2O_2 as the end product. The endogenous generation of H_2O_2 in the RAW 264.7 cells induced by PMA was evaluated and the flux of H_2O_2 releasing from the cells was measured with the use of the developed

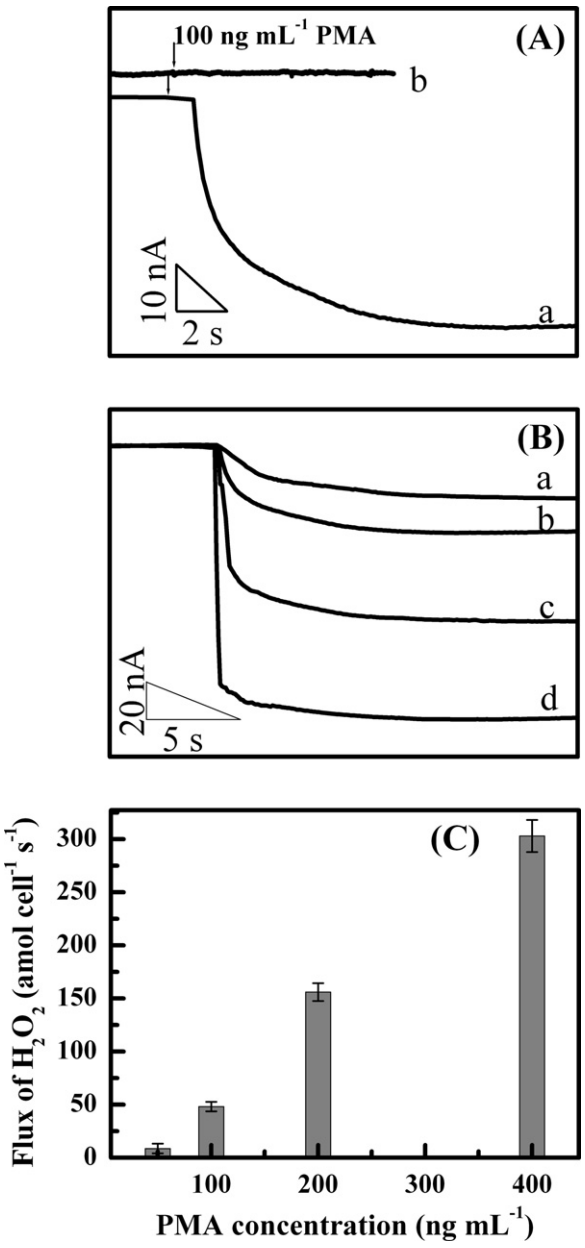

Fig. 4. (Panel A), typical amperometric responses of the HRP-attapulgite/GC electrode for the reduction of H_2O_2 released from RAW 264.7 macrophage cells induced by PMA (100 ng mL^{-1}) with (curve b) and without (curve a) addition of 50 μL of catalase (300 U mL^{-1}). (Panel B), the time course of H_2O_2 released from the cells induced by 50 (a), 100 (b), 200 (c), and 400 ng mL^{-1} of PMA (d). (Panel C) Dependence of the flux of H_2O_2 releasing from the cells on the concentration of PMA.

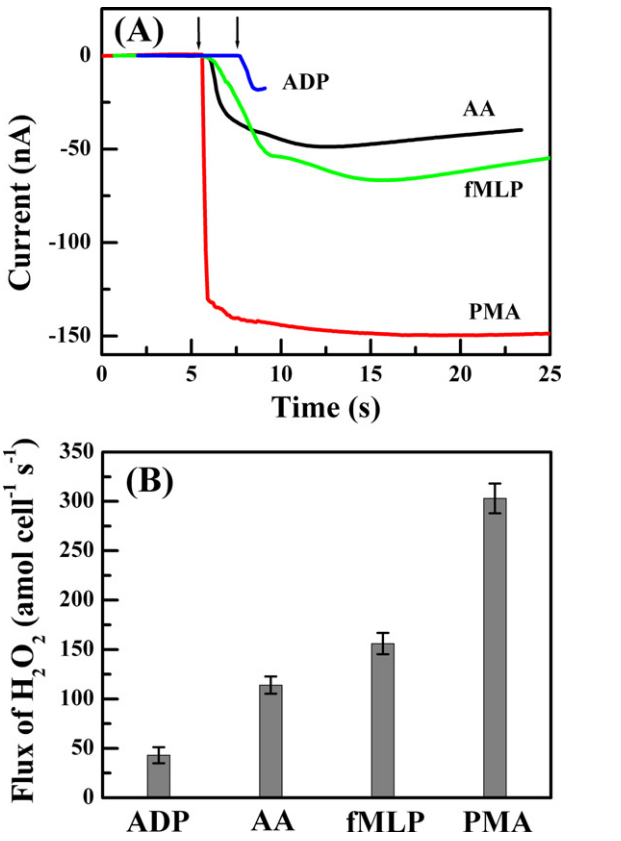

Fig. 5. The time course (panel A) and the flux of H_2O_2 (panel B) released from the cells induced by 400 ng mL^{-1} ADP, AA, fMLP, and PMA, respectively. The arrow indicates the addition of stimuli.

electrode by amperometry since this technique can provide much more precise kinetic information on the exocytotic process itself and allows evaluation in real-time of the whole efficiency of the exocytotic process (Amatore et al., 2008; Borgmann, 2009).

Curve (a) in Fig. 4 (panel A) depicts amperometric response obtained at the HRP-attapulgite/GC electrode located near the cell in PBS (pH 7.4) at a detection potential of −400 mV. After a very short period (less than 2 s) upon injection of PMA, the response increases suddenly (curve a, panel B in Fig. 4), indicative of a large amount of H_2O_2 releasing from the cells through the expansion of the fusion pore (Chow et al., 1992; Amatore et al., 2005; Amatore et al., 2008). Then a stable current reaches featuring the end of the event. The current decays gradually to zero within ca. 200 s (not shown here), indicating H_2O_2 releasing from the cells has been completely consumed or diffused away from the electrode surface. To verify the response depicted in curve a (panel A, Fig. 4) is only due to the response of H_2O_2 releasing from the cells, 50 μL of catalase solution (300 U mL^{-1}), which was known as a selective scavenger of H_2O_2 (Szymczyk et al., 2006), were injected into the solution before the addition of PMA. The response of H_2O_2 at the electrode disappears (curve b, panel A in Fig. 4) since the releasing H_2O_2 was scavenged by catalase, demonstrating that the addition of PMA can only induce the release of H_2O_2 from the RAW 264.7 cells and cannot lead to the release of other ROS or RNS. Otherwise, the response of the electrocatalytic reduction of other ROS such as O_2 at the electrode should be observed because catalase cannot scavenge O_2. A maximum current of (47.3 ± 1.6) nA is obtained at ca. 17 s after injection of PMA. This current corresponds to the H_2O_2 amount of (8.2 ± 0.5) nmol, which was calculated based on the calibration curve depicted in inset (A) of Fig. 3. Therefore, the mean flux of H_2O_2 releasing from the cells is evaluated to be (48.2 ± 2.9) amol cell^{-1} s^{-1}. These results suggest that the developed biosensor could be useful in determination of cellular H_2O_2.

The effects of PMA loading on the amount of H_2O_2 generated in RAW264.7 cells and the flux of the H_2O_2 releasing from the cells can also be studied using the developed method. Panel B in Fig. 4 depicts the time course of H_2O_2 releasing from the cells induced by different concentration of PMA. The release rate of H_2O_2 is enhanced by the increase of PMA loading as reflected by the slope of the curve (a) to (d) (panel B) in the rising periods, demonstrating the exocytosis develops rapidly with stimulation of large amount of PMA. Moreover, the amount of H_2O_2 releasing from the cells significantly increases with enhancement of the PMA loading. The mean flux of H_2O_2 from the cells also increases with the increasing of PMA concentration

(panel C in Fig. 4), showing a PMA concentration-dependent manner.

The developed electrode can be also used for measuring the flux of H_2O_2 releasing from the cells induced by a variety of stimuli such as fMLP, ADP, and AA, which were reported to induce the generation of H_2O_2 in cells (He et al., 2008; Kim et al., 2010). The amount of H_2O_2 generated in the cells and the flux of H_2O_2 from the cells are significantly dependent on the stimuli (Fig. 5). The amount of H_2O_2 generated in the cells increases in the order of ADP, AA, fMLP, and PMA (each at the concentration of 400 ng mL^{-1}, panel A in Fig. 5). The results presented in Fig. 5 also demonstrate that the cells response rapidly to the stimulation, and the generation and the release of H_2O_2 from the cells are fast. Accordingly, the flux of the H_2O_2 from the cells is also dependent on the stimuli. The maximum flux is obtained when PMA is used as a stimulator, and the flux is the lowest in the case of ADP (panel B in Fig. 5). Therefore, the developed electrode could be used for studying the H_2O_2 generation in cells as well as quantifying the flux of H_2O_2 releasing from cells. These observations substantially demonstrate that the developed electrode represents a new biosensing platform for a reliable collection of kinetic information of cellular H_2O_2 release and could be potentially useful for oxidative stress biosensors in study of downstream biological effects of various stimuli in physiology and pathology.

4. Conclusions

In summary, a new amperometric H_2O_2 biosensor based on the assembly of HRP on the surface of natural mineral attapulgite nanostructures has been developed. The biosensor exhibited a fast response, a broad linear range, a low detection limit with satisfactory stability and repeatability and could be used for the studying the kinetic of the release process and measuring the flux of H_2O_2 from the cells. The fabrication method of the biosensor has many advantages such as use of natural mineral as immobilization substrate, ease of fabrication, enhanced electrocatalysis, efficiently preserving the activity of enzyme molecules, and effective discrimination to the common coexisting ROS and RNS.

Acknowledgements

This work is supported by the National Natural Science Foundation of China (20773067, 20833006, and 20905036), Research Fund for the Doctoral Program of Higher Education of China (20103207110004), the Foundation of the Jiangsu Education Committee (09KJA150001, 09KJB150006 and 10KJB150009), and the Foundation of Jiangsu Provincial Key Laboratory of Palygorskite Science and Applied Technology (HPK201005).

Appendix A. Supplementary data

Supplementary data associated with this article can be found, in the online version, at doi:10.1016/j.bios.2011.03.018.

References

Amatore, C., Arbault, S., Bonifas, I., Bouret, Y., Erard, M., Ewing, A.G., Sombers, L.A., 2005. Biophys. J. 88, 4411–4420.
Amatore, C., Arbault, S., Guille, M., Lemaître, F., 2008. Chem. Rev. 108, 2585–2621.
Amatore, C., Arbault, S., Koh, A.C.W., 2010. Anal. Chem. 82, 1411–1419.
Bartosz, G., 2006. Clin. Chim. Acta 368, 53–76.
Borgmann, S., 2009. Anal. Bioanal. Chem. 394, 95–105.
Cai, C.X., Chen, J., 2004. Acta Chim. Sinica 62, 335–340.
Cao, Z.J., Jiang, X.Q., Xie, Q.J., Yao, S.Z., 2008. Biosens. Bioelectron. 24, 222–227.
Carlsson, G.H., Nicholls, P., Svistunenko, D., Berglund, G.I., Hajdu, J., 2005. Biochemistry 44, 635–642.
Chang, M.C.Y., Pralle, A., Isacoff, E.Y., Chang, C.J., 2004. J. Am. Chem. Soc. 126, 15392–15393.
Chen, D.X., Wang, Q., Jin, J., Wu, P., Wang, H., Yu, S.Q., Zhang, H., Cai, C.X., 2010. Anal. Chem. 82, 2248–2455.
Chow, R.H., Vonruden, L., Neher, E., 1992. Nature 356, 60–63.
Dickinson, B.C., Huynh, C., Chang, C.J., 2010. J. Am. Chem. Soc. 132, 5906–5915.
DiMauro, S., Schon, E.A., 2008. Annu. Rev. Neurosci. 31, 91–123.
Droge, W., Schipper, H.M., 2007. Aging Cell 6, 361–370.
Finkel, T., 2000. FEBS Lett. 476, 52–54.
Finkel, T., Serrano, M., Blasco, M.A., 2007. Nature 448, 767–774.
Gorton, L., Jönsson-Pettersson, G., Csöregi, E., Johanson, K., Domínguez, E., Marko-Varga, G., 1992. Analyst 117, 1235–1241.
He, W.F., Liu, G., Chen, X., Lu, J.C., Abe, H., Huang, K.X., Manabe, M., Kodama, H.J., 2008. J. Agric. Food Chem. 56, 1921–1927.
Huang, J.-L., Tsai, Y.-C., 2009. Sens. Actuators B: Chem. 140, 267–272.
Kim, G., Lee, Y.E.K., Xu, H., Philbert, M.A., Kopelman, R., 2010. Anal. Chem. 82, 2165–2169.
Kojima, H., Nakatsubo, N., Kikuchi, K., Kawahara, S., Kirino, Y., 1998. Anal. Chem. 70, 2446–2453.
Ledru, S., Ruillé, N., Boujtita, M., 2006. Biosens. Bioelectron. 21, 1591–1598.
Li, X.G., Liu, Y., Zhu, A.W., Luo, Y.P., Deng, Z.F., Tian, Y., 2010. Anal. Chem. 82, 6512–6518.
Lin, Q.Y., Jin, L.J., Cao, Z.H., Lu, Y.N., Xue, H.Y., Xu, Y.P., 2008. Phytoether. Res. 22, 740–745.
Lindgren, A., Ruzgas, T., Gorton, L., Csöregi, E., Ardila, B.G., Sakharov, Y.I., Gazaryan, I.G., 2000. Biosens. Bioelectron. 15, 491–497.
Luo, Y.P., Liu, H.Q., Rui, Q., Tian, Y., 2009. Anal. Chem. 81, 3035–3041.
Meng, L., Wu, P., Chen, G.X., Cai, C.X., Sun, Y.M., Yuan, Z.H., 2009a. Biosens. Bioelectron. 24, 1751–1756.
Meng, L., Yang, L.G., Zhou, B., Cai, C.X., 2009b. Nanotechnology 20 (035502), 8.
Miao, S.D., Leeman, H.G., Feyter, S.D., Schoonheydt, R.A., 2010. Chem. Eur. J. 16, 2461–2469.
Miller, E.W., Tulyathan, O., Isacoff, E.Y., Chang, C.J., 2007. Nat. Chem. Biol. 3, 263–267.
Neaman, A., Singer, A., 2000. Soil Sci. Soc. Am. J. 64, 427–436.
Ohshima, H., Tatemichi, M., Sawa, 2003. T. Arch. Biochem. Biophys. 417, 3–11.
Peng, Y., Jiang, D.L., Su, L., Zhang, L., Yan, M., Du, J.J., Lu, Y.F., Liu, Y.N., Zhou, F.M., 2009. Anal. Chem. 81, 9985–9992.
Rossi, D.J., Jamieson, C.H.M., Weissman, I.L., 2008. Cell 132, 681–696.
Sevanian, A., Hochstein, P., 1985. Annu. Rev. Nutr. 5, 365–390.
Shan, D., Li, Q.-B., Ding, S.-N., Xu, J.-Q., Cosnier, S., Xue, H.-G., 2010. Biosens. Bioelectron. 26, 536–541.
Simons, K., Toomre, D., 2000. Nat. Rev. Mol. Cell Biol. 1, 31–39.
Szymczyk, N.H., Kerr, B.A.E., Freeman, T.A., Adams, C.S., Steinbeck, M.J., 2006. Biochem. Pharmacol. 72, 761–769.
Troll, W., Wiesner, R., 1985. Annu. Rev. Pharmacol. Toxicol. 25, 509–528.
Wang, B., Zhang, J.J., Pan, Z.Y., Tao, X.Q., Wang, H.S., 2009. Biosens. Bioelectron. 24, 1141–1145.
Wang, J.H., Li, L.M., Huang, W.H., Cheng, J.K., 2010. Anal. Chem. 82, 5380–5383.
Welinder, K.G., 1979. Eur. J. Biochem. 96, 483–502.
Wu, X.M., Hu, Y.J., Jin, J., Zhou, N.L., Wu, P., Zhang, H., Cai, C.X., 2010. Anal. Chem. 82, 3588–3596.
Xhattopadhyay, K., Mazumdar, S., 2000. Biochemistry 39, 263–270.
Xu, H., Aylott, J.W., Kopelman, R., 2002. Analyst 127, 1471–1477.
Yang, X.S., Chen, X., Yang, L., Yang, W.S., 2008. Bioelectrochemistry 74, 90–95.
Yang, H.M., Yang, A.D., Ouyang, J., Li, M., Mann, S., 2010. J. Phys. Chem. B 114, 2390–2398.
Ye, F.G., Huang, Y., Xu, Q., Shi, M., Zhao, S.L., 2010. Electrophoresis 31, 1630–1636.